A numerical investigation of the compressible flow in the ejector of a vapour ejector refrigeration system

A. Megalingam and V. Babu*

Department of Mechanical Engineering,
Indian Institute of Technology Madras,
Chennai 600036, India
Email: megalingamarumugam@gmail.com
Email: vbabu@iitm.ac.in
*Corresponding author

Abstract: Numerical simulations of the flow in a vapour ejector have been carried out. Real gas effects are accounted for in the calculations. Ejection as well as flow-through studies have been performed. Effects of the generator and evaporator temperatures and position of the primary nozzle have been investigated. Predicted values of the suction pressure and COP have been compared with experimental values reported in the literature. In addition, secondary flow area has also been evaluated and correlated with the COP. By tracking the sonic line and the edge of the primary stream and flow separation, insights on the gas dynamic and fluid dynamic aspects of the flow field and how they influence the entrainment of the secondary stream and consequently the COP are brought out. The study reveals that, in addition to the choking of the secondary stream, the expansion of the primary stream and the area available for the secondary stream also plays a key role in affecting the performance of the vapour ejector.

Keywords: numerical simulation; ejector; real gas effects; solar refrigeration.

Reference to this paper should be made as follows: Megalingam, A. and Babu, V. (2020) 'A numerical investigation of the compressible flow in the ejector of a vapour ejector refrigeration system', *Progress in Computational Fluid Dynamics*, Vol. 20, No. 1, pp.29–39.

Biographical notes: A. Megalingam is currently a Graduate Engineer Trainee at Thermax, Pune, India. He completed his BTech in Mechanical Engineering from the National Engineering College, Tamilnadu and joined the Indian Institute of Technology for his MS in 2015.

V. Babu received his PhD from the Ohio State University in 1991. He worked as a Technical Specialist at the Ford Research Lab in Dearborn, Michigan from 1995–1998. He joined the Indian Institute of Technology Madras in 1998 as an Assistant Professor and is currently a Professor.

1 Introduction

The vapour ejector refrigeration system (Little and Garimella, 2011) is an attractive and viable alternative to vapour compression refrigeration systems for rural applications owing to its design simplicity and utilisation of low grade energy such as waste heat from industries, power plants or solar thermal energy. In addition, the pump in this system may be run using solar PV, thus eliminating the need for grid connectivity. However, as is well known the COP of the ejector refrigerator system is quite low.

Research has been going on in the past to study the effect of working fluid, operating condition and combination with other cycles on the performance of the ejector refrigeration system. Furthermore, studies have focussed on the design and operation of ejectors using air, steam and refrigerant as the working fluid. A comprehensive review of the literature on vapour ejector refrigerator system has been given by Little and Garimella (2011). As the focus of the present study is on the gas dynamic aspects of the flow through the ejector, a brief discussion of the recent literature related to this aspect is presented next.

Arbel et al. (2003) studied the irreversibilities in the ejector by analytically evaluating the entropy production. Irreversibilities due to pure mixing, kinetic energy losses and normal shock wave were evaluated. They reported that irreversibility due to pure mixing can be eliminated by proper selection of fluid and inlet conditions and that an appropriate adjustable throat can eliminate losses associated with normal shock. Kinetic energy losses could be reduced but not eliminated.

Hewedy et al. (2008) conducted numerical and experimental analysis on the optimum geometry of the air ejector. From the results, numerical formulae relating ejector geometry parameters such as the length and diameter of the mixing chamber and operating parameters were derived.

Zheng et al. (2011) numerically studied the influence of geometry on the starting vortex and ejector performance. It was suggested that the optimal mixing chamber diameter of the ejector is governed by the vortex toroid. And also the effect of the length of the ejector on the overall performance of the ejector was studied and shown to be less important than the mixing chamber diameter.

Little et al. (2015) compared shadowgraph images of the flow in an air-ejector with results of numerical simulations using turbulence models RNG $k-\omega$ and SST $k-\omega$ and an analytical model constructed from first principles. It was shown that on-design ejector operation is predicted with better accuracy than off design operation. The SST $k-\omega$ model was shown to predict the location of flow features, as well as global inlet mass flow rates, with great accuracy.

Chen et al. (2017) investigated the Mach flow structure of the driving flow under off-design working conditions both experimentally and numerically. Method of characteristics was used for the numerical calculations whereas Schlieren imaging was used in the experimental study. Expansion wave from the driven flow was shown to affect the ejector performance.

Ramesh and Sekhar (2018) conducted an experimental study of the effect of suction chamber angle on the entrainment of passive fluid in a steam ejector. An optimum angle for the suction chamber increased entrainment ratio by 49.96% but had a minor influence on the back pressure.

Bartosiewicz et al. (2005) reported results from numerical and experimental investigations of ejectors using air as the working fluid. Predictions obtained using the ideal gas approximation and six different turbulence models were compared against experimentally determined shock location, shock strength and pressure recovery in the absence of secondary flow. The non-mixing length was determined using laser tomography visualisation in the experiments and using a colorant in the simulations. The RNG $k-\varepsilon$ and the SST $k-\omega$ models were seen to give the best predictions. The latter was then used for further calculations under on- and off-design operating conditions. It was shown that the secondary flow must get choked in the mixing chamber in order to achieve a high entrainment ratio.

Yapici and Yetisen (2007) experimentally investigated a vapour ejector refrigeration system with R11 as the working fluid. The effect of the generator temperature, condenser pressure and the evaporator temperature on the COP and the cooling capacity were studied systematically. Both these quantities increased with the generator temperature and evaporator temperature. They remained constant as the condenser pressure was increased until a threshold value was reached, after which they decreased steeply.

Yapici (2008) carried out an experimental study to determine the optimum position of the primary nozzle with respect to the mixing chamber entrance. It was reported that suction chamber pressure (in the absence of secondary flow) was a minimum (indicating good ejection action) when the primary nozzle exit was located a distance of $x/d_{th} \leq 2$ beyond which the performance deteriorated sharply. This was consistent with the findings reported earlier by Nahdi et al. (1993). Experiments with the secondary flow enabled were then carried out with the primary nozzle kept at this optimum position.

Hemidi et al. (2009) simulated single phase (air, assumed to be ideal) and two phase flows (air and water droplet) in an ejector with SST $k-\omega$ and $k-\varepsilon$ turbulence models. Comparison with experimental results showed predictions to be higher by 10–20% and 10% respectively. However, the former predicted the shock cells much better than the latter. They also suggested that the sonic line be used to relate the flow features to the entrainment ratio.

Zhu et al. (2009) simulated R141b ejectors to find out the effect of primary nozzle exit position (NXP) and mixing chamber convergence angle on the entrainment ratio. Three different turbulence models, namely, the Realisable $k-\varepsilon$, RNG $k-\varepsilon$ and SST $k-\omega$ were used along with the ideal gas approximation. The predictions of the RNG $k-\omega$ model were found to be better than the other two and this was used for the subsequent production runs of 95 ejector geometries. The optimum primary nozzle position was found to be proportional to the mixing chamber diameter and it increased with a rise in the primary flow pressure. A less than optimum primary nozzle position was seen to cause reduced energy transfer while a higher primary nozzle position led to increased friction and kinetic energy losses. The entrainment ratio became less sensitive to the convergence angle of the mixing chamber with increasing nozzle position.

Chandra and Ahmed (2014) reported results from the experimental and numerical investigations of ejectors. Steam was used as the working fluid in the experiments whereas air (assumed to be ideal) was used in the simulations. Constant area as well as varying area mixing chambers were investigated. The entrainment ratio was shown to increase with the generator temperature up to a certain value beyond which there was a sharp decrease. This sudden decrease was attributed to the blocking of the of the flow passage by the over-expanded flow from the primary nozzle.

Wu et al. (2014) performed axi-symmetric simulations of steam ejectors used in desalination applications using the Realisable $k-\varepsilon$ model. The length and convergence angle of the constant pressure mixing chamber were selected as parameters for this study. It was found that there existed a range of optimum mixing chamber length, in which the entrainment ratio was a maximum and nearly constant. In shorter mixing chambers, due to double choking phenomenon (Munday and Bagster, 1977), a normal shock was located at the mixing chamber outlet. The shock became weaker and the entrainment ratio reached a maximum with increasing mixing chamber length. Eventually, the double choking and normal shock both disappear and the entrainment ratio falls drastically. A theoretical analysis of ejector design and ejector cycle performances was carried out by Shestopalov et al. (2015). 1D model was developed for ejectors with cylindrical mixing chambers or conical-cylindrical mixing chambers.

Geometric parameters of ejectors for maximum entrainment ratios were derived by an optimisation procedure. It was shown that the conical-cylindrical mixing chamber design performed better.

Based on the available literature, it emerges that analytical investigations are limited by the simplifications necessary in order to make the problem tractable to closed form solutions. On the other hand, experimental studies have not been able to provide detailed information on the flow field inside the ejector when the working fluid is not air. Hence, the objective of the present study is to gain insights into the gas dynamic aspects of the flow of a refrigerant in the ejector through numerical simulations. To this end, the vapour ejector system investigated experimentally by Yapici (2008) has been chosen for the simulations. Salient features of the present study are:

1 the primary and the secondary fluid are both refrigerants and not air or steam

2 real gas effects are fully accounted for.

Novel aspects of the present work in comparison to the computational studies mentioned earlier are:

1 prediction of the suction chamber pressure, which is an important performance metric (Little and Garimella, 2011) and the corresponding flow field, for different primary nozzle positions

2 insights on the effect of the gas dynamic aspects of the flow field on the COP, such as, the importance of the area available for the secondary flow on the overall performance.

2 Formulation and solution methodology

2.1 Problem description and solution domain

The ejector geometry considered here is shown in Figure 1. High enthalpy fluid from the generator is accelerated to supersonic speeds by the convergent divergent nozzle (referred to as the primary nozzle). This high speed flow (termed the primary flow) entrains the fluid in the suction chamber thereby creating a flow (termed the secondary flow) of the low enthalpy fluid from the evaporator into the suction chamber. These two streams mix in the mixing chamber and the resulting fluid of intermediate enthalpy and pressure is diffused before it enters the condenser (Figure 2). The degree of mixing determines the effectiveness of the device and this is evaluated using metrics such as the ratio of the static pressures or static enthalpies or mass flow rates across the ejector (Little and Garimella, 2011).

It is clear from the sketch on the top in Figure 1 that the geometry is rendered three-dimensional by the inlet from the evaporator. However, the geometry downstream of the inlet is axi-symmetric and this has been advantageously taken to be the computational domain in the present study (Figure 1). The domain itself is split into two sub-domains, namely, the primary nozzle (bounded by *a-b-c-d* in Figure 1) and the ejector (bounded by *c-e-f-g-h-d* in Figure 1). During operation, the flow is choked at the throat of the primary nozzle and in addition, it is also supersonic in the entire divergent portion. Therefore, it is computationally quite expedient to simulate the flow in the nozzle separately and impose the conditions computed at the nozzle exit as inlet conditions for the ejector. An added advantage of this strategy is that, as the nozzle is moved to different axial locations, the flow in the nozzle need not be computed again. Only the flow in the ejector with the nozzle exit at the new location needs to be simulated again.

Figure 1 (a) The ejector geometry experimentally studied by Yapici (2008) (b) The computational domain used in the present study

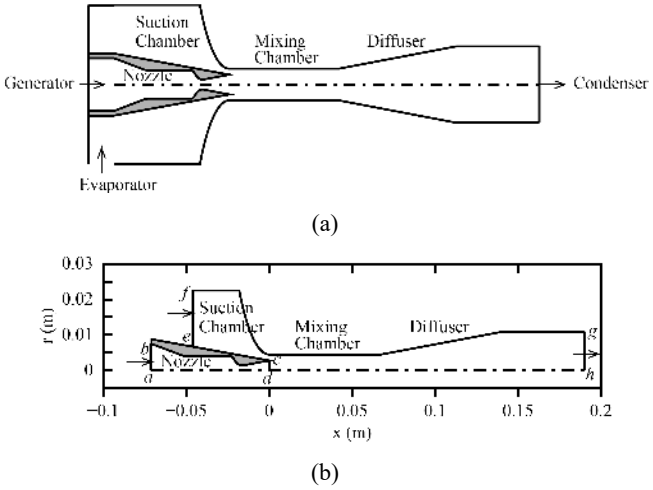

Figure 2 *P – h* diagram of the ejector refrigeration cycle

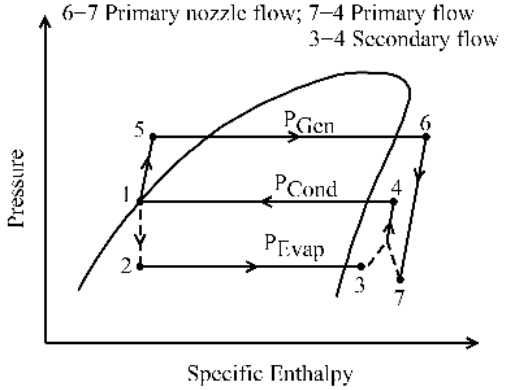

2.2 Governing equations and modelling

The flow under consideration is axi-symmetric, compressible, mixed subsonic-supersonic and also turbulent owing to the high speeds. Accordingly, the axi-symmetric form of the Favre averaged NS equations are solved (Wilcox, 1994). Turbulence has been modelled using the SST $k - \omega$ model with compressibility effects included and with default values for the constants. This has been shown to give reasonably good predictions in earlier studies (Little et al., 2015; Bartosiewicz et al., 2005; Hemidi et al., 2009). An implicit second order accurate upwind scheme has been used for spatial discretisation of the governing equations.

All the results presented here have been obtained using ANSYS FLUENT 14.5.

The fluid considered here is refrigerant R123, since the same was used in the experiments by Yapici (2008). In order to clearly bring out the real gas effect on the flow field, the calculations have been carried using the ideal gas as well as the real gas model. For the latter, the modified Benedict-Webb-Rubin equation of state is used with property values being evaluated from the REFPROP v7.0 NIST database.

2.3 Boundary conditions

Specification of proper boundary conditions for the numerical simulations is made difficult in the present case on account of the fact that:

a these conditions have to mimic the conditions that prevailed during the experiments

b the required values at the computational boundaries may not be readily available.

2.3.1 Primary nozzle

For the primary nozzle flow simulations, the nozzle inlet (labelled *a–b* in Figure 1) is modelled as a subsonic pressure inlet, where the stagnation pressure and stagnation temperature are specified. Ideally these values should be the same as those in the generator. However, there would definitely have been a pressure drop in the experimental setup between the generator and the nozzle inlet due to friction in the line connecting the two. Owing to the absence of any information regarding this aspect, in the present work, the pressure drop has been assumed to be 0.1 bar. If isenthalpic flow is assumed in the line then the exit temperature may be calculated. This comes out to be almost the same as the generator temperature.

The wall of the nozzle (labelled *b–c* in Figure 1) is assumed to be an adiabatic, no-slip surface. Since the flow is supersonic at the exit (labelled *c–d* in Figure 1), no values may be prescribed here and all the variables are evaluated from the interior by second order accurate extrapolation. Boundary segment *a–d* is treated as an axis of rotation.

Figure 3 Mass flow rate in the primary nozzle for different generator temperatures

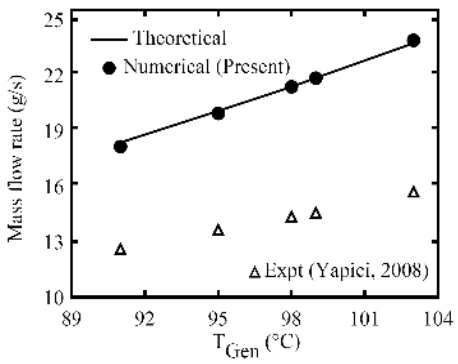

Results from nozzle calculations using the procedure described above predict the mass flow rates in the primary nozzle to be within 1% of the theoretical value for choked isentropic flow in a nozzle, for the range of generator temperature investigated in the experiment (Figure 3). However, these values are around 25% higher than the experimentally reported values. This discrepancy did not decrease even after doubling the number of nodes in the axial and radial directions. Hence, calculations were attempted by modelling the nozzle inlet as a mass flow inlet where the mass flow rate (which is known from the experiment) and stagnation temperature (same as generator temperature) are specified. However, the stagnation pressures at the nozzle inlet were predicted to be 15–28% less than the generator pressure, which is unreasonable. The only way to reconcile these conflicts is to reduce the nozzle throat diameter. This was confirmed by running the calculations with the nozzle diameter reduced (after several trials) to 2.35 mm from 2.85 mm. The resulting mass flow rate agreed with the experimental value to within the measurement error of 4.3% for all the generator conditions considered here. However, such a change significantly affects the gas dynamics of the flow for the following reasons:

a the reduced throat diameter increases the exit to throat area ratio and hence the exit Mach number

b the reduced throat diameter will have a cascading effect on all the other dimensions resulting in large changes in the ejector geometry.

Consequently, all the results presented here have been obtained by modelling the nozzle inlet as a pressure inlet with the throat diameter equal to 2.85 mm.

2.3.2 Ejector

Boundary segment *c–d* is modelled as a pressure inlet with the values obtained from the nozzle calculations being prescribed here. Since the node distributions are different between the nozzle outlet boundary and the pressure inlet boundary, a second order accurate interpolation procedure is used for transferring the values from the former to the latter. Boundary segment *e–f* is modelled as a no-slip, adiabatic wall for calculations with no secondary flow. Otherwise, it is modelled as a pressure inlet with the stagnation pressure and stagnation temperature being set to the evaporator pressure and temperature respectively. Boundary segment *f–g* is modelled as a no-slip, adiabatic wall, *d–h* is modelled as an axis and *g–h* is modelled as a pressure outlet with the exit static pressure specified to the same as the condenser pressure.

2.4 Convergence metrics

Convergence of the numerical calculations is assessed through mass, momentum and energy balance between the inlet(s) and the outlet of the computational domain. Momentum balance is checked by evaluating the left and

right hand sides of the following expression separately and then computing the difference.

$$F_{wall} = \left[\int_0^R \left(P + \rho u_x^2\right) 2\pi r dr\right]_{inlet}^{outlet}$$

The left hand term is the net force acting on the walls (pressure + viscous) in the x-direction. The right hand term is the change in the impulse function of the fluid between the inlet(s) and the outlet. For all the results presented here, these balances are satisfied to less than 4% for mass and 5% for the other two. It is worth noting that the experimental uncertainty in the mass flow measurement is 4.3%.

2.5 Grid independence study

In addition to ensuring the convergence metrics mentioned previously, it is essential to establish grid independence of the results for them to be acceptable.

The primary nozzle geometry has been meshed using a structured mesh with 300 points and 40 points in the axial and radial directions respectively. The wall y+ in the nozzle flow field is everywhere less than 60. This is acceptable, since the use of the standard wall function at the no-slip surfaces requires this value to be less than 100. Axial gradients are also resolved very well with clustering of the mesh points in the throat region and so this mesh was deemed to be adequate as the flow is supersonic in the divergent portion of the nozzle and devoid of any shock. Doubling the grid points in both the axial and radial directions did not show any discernable change in the predicted quantities at the primary nozzle exit.

The ejector domain has been meshed using a multi-block body mesh. The suction chamber has been meshed with a body fitted non-uniform mesh. The mesh is fine near the throat section since this is the region of intense mixing between the primary and the secondary flow. The baseline mesh has 700, 450 and 350 nodes along the axial direction in the mixing chamber, diffuser and the constant area sections respectively and 43 nodes in the radial direction. The axial distribution of the nodes and the variation of the static pressure along the axis and the wall are shown in Figure 4. It may be inferred from the static pressure distribution that the number of nodes is unnecessarily high in the diffuser and the constant area section. Consequently, two more meshes, namely, an intermediate one with 1,100, 300 and 100 nodes and a fine mesh with 1,300, 150 and 50 nodes are generated. The axial distribution of the nodes in these two meshes is shown in Figure 4. It can be seen that a large number of nodes are concentrated in the mixing region just downstream of the nozzle exit where the gradients are steep. It must also be noted that the total number of nodes has been kept the same for all three meshes. The variation of static pressure along the axis and the wall for the intermediate and the fine meshes are also shown in Figure 4. The change in the wall static pressure is less than 0.048% between the baseline and the intermediate mesh results and 0.039% between the intermediate and the fine mesh results. The change in the static pressure along the axis between the baseline and the intermediate mesh results is less than 3.29% and that between the intermediate and fine mesh results is less than 0.62%. Although it appears that the intermediate mesh itself is adequate, the fine mesh has been used for all the calculations. The highest value for the wall y^+ in the fine mesh is 80 which indicates that the near wall resolution in the radial direction is also acceptable.

Figure 4 Variation of static pressure along (a) the axis and (b) the top wall (c) Distribution of the nodes along the axial direction for different grids

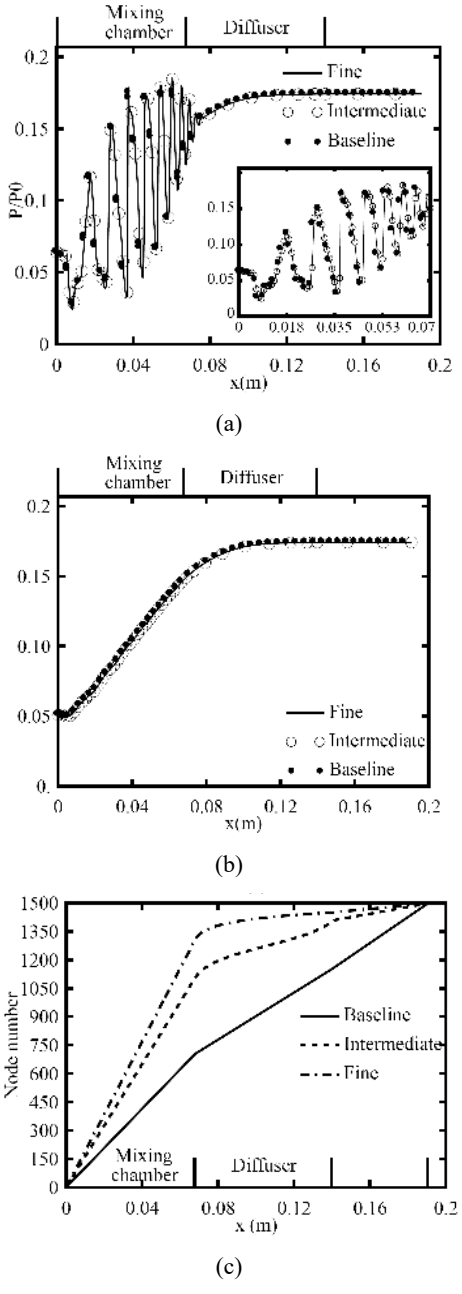

Notes: Baseline results are shown for every 30th node, and the intermediate results are shown for every 35th node, for the sake of clarity. Inset shows a close-up view in regions of steep gradient with results shown for every 15th node for the baseline and intermediate meshes.

3 Results

Results from numerical calculations are presented in this section under two broad categories: ejection study, wherein boundary segment *e–f* is treated as a wall; flow through study, wherein this boundary segment is treated as an inlet boundary (with fluid entering at the evaporator exit conditions). In addition to these two, results are also presented to highlight real gas effects on the flow field predictions. The condenser pressure has been set equal to 125 kPa for all the cases reported here.

3.1 Ejection study

Ejection simulations have been carried out for four nozzle positions with the nozzle exit located at x = 0 mm, –18 mm, –30 mm and –36 mm. The simulations are started with the pressure in the suction chamber set to a certain value. The calculations are terminated when the ejection action tapers off and the convergence metrics mentioned earlier are satisfied. The final pressure in the suction chamber is referred to as the suction pressure. In order to check the dependence of the predicted value of the suction pressure on the initial value, simulations have been run with different initial values, namely, 70 kPa, 100 kPa and 125 kPa. Furthermore, simulations have also been run with an extended computational domain by including the entire suction chamber used in the experiments by Yapici (2008), in order to determine the sensitivity of the predicted suction pressure to the suction chamber volume. The predictions have been found to be insensitive to the chamber volume but exhibit a variation of 15% or less based on the initial chamber pressure. All the results presented here have been obtained with the initial pressure set to 100 kPa and with the chamber geometry shown in the bottom in Figure 1.

Figure 5 Variation of suction pressure for different nozzle positions with T_{Gen} = 98°C

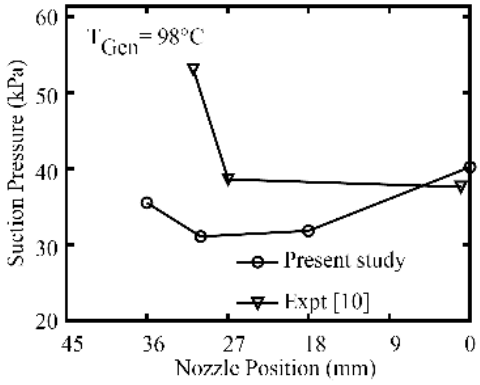

Numerically predicted values of the suction chamber pressure for different primary nozzle positions and generator temperature, T_{Gen} = 98°C are plotted in Figure 5. Experimental values reported by Yapici (2008) are also shown in this figure for comparison. It can be seen that, experiments showed the 0 mm nozzle position to be the optimum whereas the present simulations show 18 mm and 30 mm nozzle positions to be even better.

In order to understand this trend in the predicted value of suction pressure, the mass entrainment ratio (MER), defined as Little and Garimella (2011):

$$MER = \frac{\dot{m}_{entrained}}{\dot{m}_{primary}} \tag{1}$$

is evaluated. Values of MER at different instants during the ejection simulation are shown for three nozzle positions in Figure 6 for T_{Gen} = 98°C. It should be noted that the starting transient values are not shown here. For all nozzle positions, the entrained stream is choked to begin with and then unchokes at an intermediate instant. This is indicated in Figure 6 by using a change in the symbol style from filled to unfilled. It is clear from this figure that the 0 mm nozzle position has the lowest entrainment ratio throughout and is hence not optimal. The case corresponding to a nozzle position of 36 mm performs better initially but deteriorates sharply once the flow becomes unchoked. Nozzle positions of 18 mm and 30 mm (not shown in Figure 6, to avoid cluttering) show the best performance towards the end of the ejection process and are optimal.

Figure 6 Variation of MER with suction chamber pressure for various primary nozzle positions

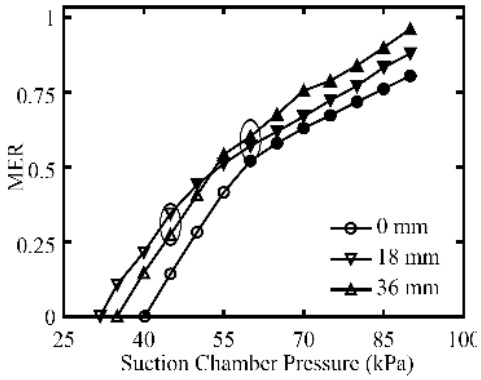

Note: Filled and unfilled symbols represent choked and unchoked entrained flows respectively.

The flow field at two instants shown circled in Figure 6, one when the suction chamber pressure is 60 kPa and one when it is 45 kPa, are shown in Figure 7, corresponding to 18 mm and 36 mm nozzle positions. It may be ascertained from Figure 6 that the flow is choked in the first instant and unchoked in the later instant for these nozzle positions. Here, the flow in the ejector is core-annular. i.e., momentum is transferred by viscous drag between the streams without any mass transfer. The streams are separated by the edge of the primary stream shown in Figure 7. Since area of the mixing chamber is constant, the mass flow rate of the secondary stream is dependent upon the mixing chamber area unfilled by the primary stream and the momentum transfer.

Figure 7 Sonic lines and primary stream edges for (a, c) 18 mm nozzle position and (b, d) 36 mm nozzle position

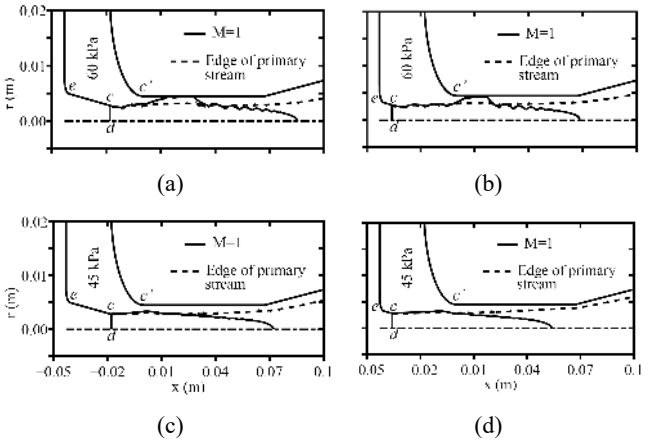

The primary stream is supersonic at the exit of the primary nozzle with Mach number equal to 2.36 and becomes subsonic farther down due to mixing. The sonic line is plotted in Figure 7 in order to delineate the subsonic and supersonic regions. The supersonic region of the primary stream plays the main role in momentum transfer and ejection. Once the primary stream becomes subsonic, its momentum is diffused into pressure rise.

At an earlier instant when the suction pressure is high, it is evident from the sonic line that the entrained flow chokes in the mixing chamber [Figure 7(a) and 7(b)] and the minimum flow area available for the entrained stream is the same for both nozzle positions. Since the distance *c–c′* is higher for the case of 36 mm nozzle position, physically there is more room for momentum transfer before entering into the mixing chamber. As a result, at the same axial position and for equal choked entrained flow area, the entrained flow of 36 mm nozzle position has higher velocity than that of 18 mm nozzle position. Hence, the 36 mm nozzle position provides higher entrainment ratio at higher suction pressures.

As the entrainment continues, the suction chamber pressure continues to decrease. Below a critical value of suction chamber pressure (the pressure at which the symbol style changes in Figure 6), the secondary stream unchokes as seen in Figures 7(c) and 7(d) for both nozzle positions. This allows the primary stream to expand. In the case of 36 mm nozzle position [Figure 7(d)], expansion of the subsonic primary stream takes place in the mixing chamber itself. This expansion causes a reduction in the available cross-sectional area for the secondary stream with an attendant reduction in the MER and the entrainment ratio becomes less than that of the 18 mm nozzle position for the same suction pressure. In the latter case, it is evident from Figure 7(c) that the expansion of primary stream takes place farther down in the diffuser where the cross-sectional area is more.

In the case of 0 mm nozzle position, the distance *c–c′* is the shortest and hence there is no momentum transfer before entering the mixing chamber. Due to inadequate momentum transfer, MER for this nozzle position is less than that for other nozzle positions. In addition, the pressure of the entrained stream at the mixing chamber inlet is also less than that for other nozzle positions. Consequently, the pressure gradient becomes adverse earlier and as a result flow separation also occurs earlier in this case when compared to the 18 mm nozzle position [Figure 8(a)]. The separation bubble blocks the passage, and causes a reduction in entrainment and hence higher suction pressure. But in the 18 mm nozzle position case, flow separation is seen at a much lower suction chamber pressure [Figure 8(b)]. Thus, even though 0 mm nozzle position has the least blockage due to expansion of the primary flow, lack of momentum transfer is the reason for poor performance throughout the ejection process.

Figure 8 Flow separation during ejection corresponding to nozzle position, (a) 0 mm and (b) 18 mm

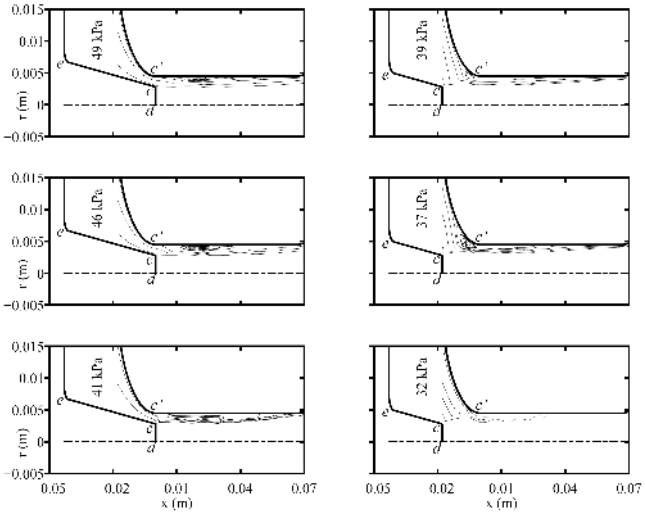

3.2 *Flow-through study*

In this case, boundary *e–f* is treated as a pressure inlet at the evaporator conditions. Calculations have been carried out for two evaporator temperatures (10°C and 15°C), four generator temperatures (91°C, 95°C, 98°C and 103°C) and three primary nozzle positions (0 mm, 18 mm and 30 mm).

The coefficient of performance (COP) is used as the performance metric. Following Little and Garimella (2011), COP is defined as

$$COP = \frac{Q_{Evap}}{Q_{Gen}} \tag{2}$$

or

$$COP = MER \frac{h_{Evap,out} - h_{Cond,out}}{h_{Gen,out} - h_{Cont,out}} \tag{3}$$

3.2.1 *Effect of the generator temperature on COP*

Predicted values of COP for a range of generator temperatures and various primary nozzle positions are compared with the results of Yapici (2008) in Figure 9. It is clear that the COP increases initially with generator

temperature and then decreases slightly. In earlier studies, it was speculated that choking of the secondary flow may cause this drop in COP. This is investigated next.

Figure 9 Variation of COP for different generator temperatures and evaporator temperatures, (a) 10°C and (b) 15°C

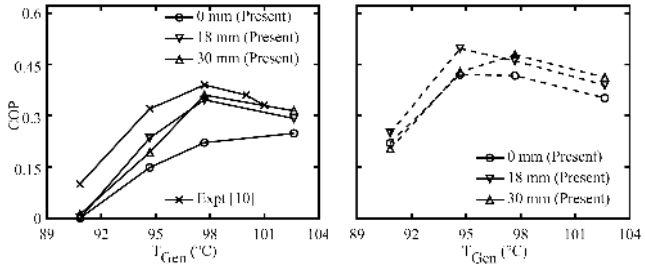

(a) (b)

At a lower value of generator temperature [Figure 10(a)], the supersonic region is of a shorter length and flow becomes subsonic within the mixing chamber itself. This high pressure subsonic primary stream expands to occupy the whole of the mixing chamber. As a result, the secondary stream is completely blocked and there is no entrainment.

Figure 10 Sonic lines and primary stream edges for 18 mm primary nozzle position and 10°C evaporator temperature for generator temperatures of (a) 91°C, (b) 95°C, (c) 98°C and (d) 103°C

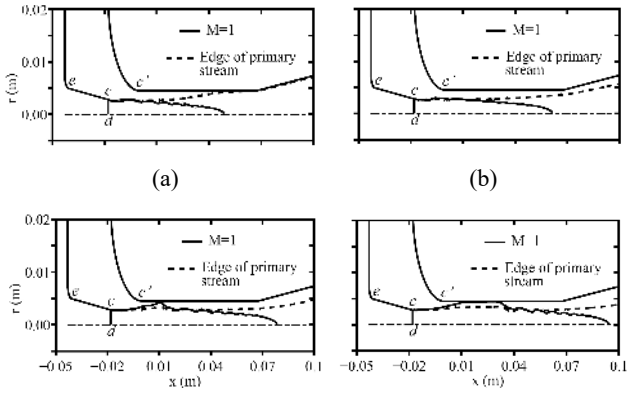

(a) (b)

(d) (d)

At a higher generator temperature [Figures 10(b) and 10(c)], the supersonic region is longer and expansion of the subsonic primary stream occurs farther downstream. When it occurs in the diffuser, which has a higher cross-sectional area than the mixing chamber, there is still sufficient area for the secondary stream to flow even after the expansion of primary subsonic stream. Hence entrainment increases with the generator temperature under these conditions.

With further increase in the generator temperature, supersonic region of the primary stream also expands near the mixing chamber inlet [Figure 10(d)]. After a particular temperature, the area occupied by the supersonic primary stream becomes significant. Due to the dragging of the supersonic primary stream and reduction in the cross-sectional area, secondary stream chokes at the mixing chamber inlet. Choking restricts further increase in the secondary mass flow rate, whereas expansion of the supersonic primary stream reduces the area of the secondary flow and secondary stream mass flow rate. These two effects cause the reduction in the COP at higher generator temperatures.

Figure 11 Predicted COPs and normalised area for secondary flow corresponding to nozzle position, (a) 0 mm (b) 18 mm (c) 30 mm

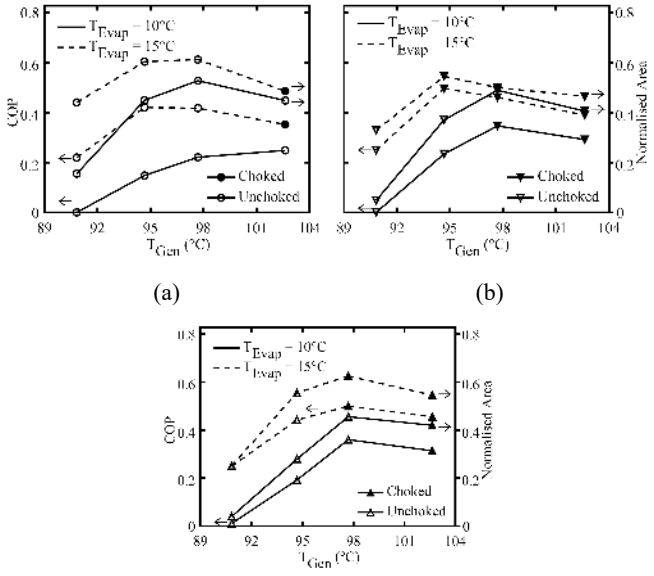

(a) (b)

(c)

It can be inferred from Figure 9 that there exists an optimum generator temperature range, in which the area occupied by the subsonic and supersonic primary regions reach a minimum and the secondary flow rate becomes a maximum. For all operating conditions studied here, predicted COP is the highest in this range. For values of temperature less than this range, the subsonic primary stream controls the flow rate of the secondary stream at the mixing chamber exit and for values higher than this range, the supersonic primary stream restricts the secondary stream flow rate at the mixing chamber inlet. This is explored in detail next. Minimum area available for the secondary flow in the mixing chamber is normalised by the mixing chamber area and the variation of this normalised area is compared with that of COP in Figure 11. It is evident that the variations are quite similar. As the generator temperature is varied, COP is affected more by the normalised area than choking. Even without choking, COP decreases due to a decrease in area for secondary flow. In three out of six combinations simulated here, reduction in COP does not coincide with the choking of the secondary flow (Figure 11).

3.2.2 Effect of the evaporator temperature on COP

An increase in the evaporator condition increases the COP for all operating conditions considered (Figure 11). An increase in the evaporator pressure increases the pressure gradient between the suction chamber and mixing chamber and hence the entrained mass flow rate increases. However, the increase in the COP at higher generator temperatures is less than that at lower generator temperature.

Figure 12 Primary stream edges for 18 mm nozzle position and generator temperatures, (a, b) 95°C (c, d) 103°C

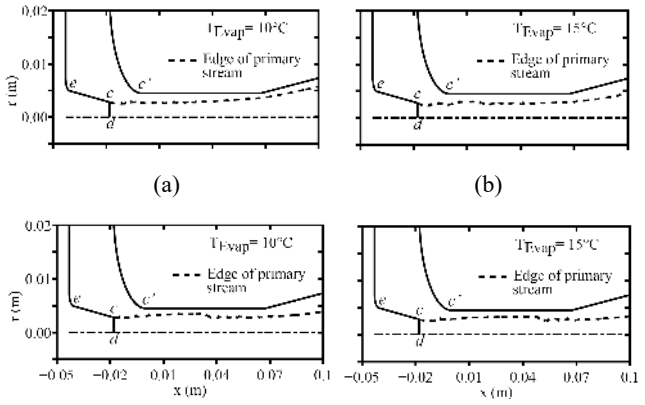

The reason for this effect is as follows. At lower generator temperatures, expansion of the primary stream at the mixing chamber exit decreases with a rise in the evaporator temperature [Figures 12(a) and 12(b)]. The increased area available for the secondary flow allows the mixing chamber to accommodate a higher secondary mass flow rate. But at higher generator temperatures, due to choking of the secondary stream, the area available for the secondary stream remains almost constant which restricts increase in entrainment and COP [Figures 12(c) and 12(d)].

3.2.3 Effect of primary nozzle position in COP

The effect of the nozzle position on the COP is dependant on the generator temperature. At a lower generator temperature (unchoked flow), pulling the nozzle back from 18 mm to 30 mm decreases the COP, whereas same movement increases the COP at higher generator temperatures.

Figure 13 Primary stream edges for 10°C evaporator temperature and nozzle positions, (a, c) 18 mm (b, d) 30 mm

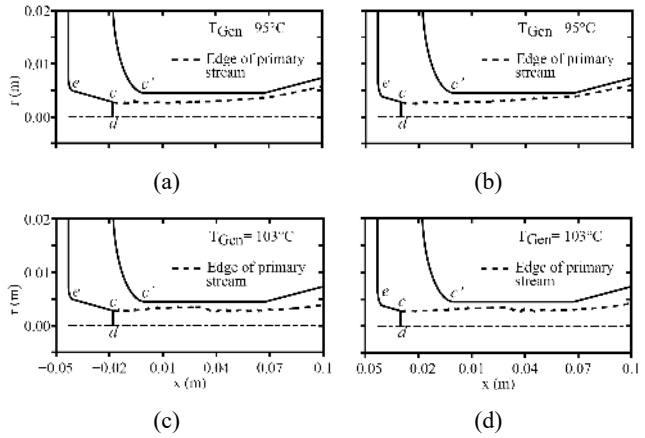

At lower generator temperatures, if the nozzle is pulled back, the subsonic primary flow starts to expand in the mixing chamber itself and reduces the area available for the secondary flow [Figures 13(a) and 13(b)]. Accordingly, 30 mm nozzle position exhibits less entrainment than 18 mm nozzle position. At higher generator temperatures, due to choking of the secondary stream, the area available for the secondary stream remains almost constant irrespective of the nozzle position [Figures 13(c) and 13(d)]. Since the distance c–c' is higher for the 30 mm nozzle position, physically there is more room for momentum transfer. Hence the secondary stream has a higher flow velocity at the inlet of the mixing chamber for 30 mm nozzle position. Accordingly, entrainment of 30 mm nozzle position is higher than that of other nozzle positions at higher generator conditions. Nozzle position of 0 mm has poor momentum transfer and COP among all the nozzle positions studied.

3.3 Comparison of ideal gas and real gas model predictions

In this study, all the simulations have been carried out with real gas and ideal gas models. For real gas simulations, Modified Benedict-Wenn-Rubin equation of state is used (Younglove and McLinden, 1994). For ideal gas simulations, values for ideal gas specific heat are taken from the same study. Compressibility factor (Z) is used as the parameter to quantify deviation from ideal gas behaviour. This is defined as

$$Z = \frac{P}{\rho RT} \tag{4}$$

where R is the particular gas constant.

For an ideal gas, compressibility factor is unity. For the range of conditions considered in the present calculations, in the mixing chamber, the maximum deviation of the compressibility factor from unity is only 4%. However inside the primary nozzle, the maximum deviation of Z from unity is predicted to be as high as 17.3% (Figure 14).

Figure 14 Contours of $|1 - Z|$ in the primary nozzle corresponding to a generator temperature of 103°C

Notes: Flow is from left to right. Contour values range from 0.18 to 0.01 in steps of 0.01 from left to right.

Primary nozzle mass flow rates and MERs of ideal gas simulations are compared with those of real gas simulations in Figure 15. Predicted primary mass flow rates from the ideal gas simulations are as much as 6.4% less than those of the real gas simulations. It can be inferred from Figure 14 that the reason for this difference is the significant departure from ideal gas behaviour in the vicinity of the throat section of the primary nozzle. However, the secondary mass flow rate remains the same for both ideal and real gas simulations.

Figure 15 Comparison of results from ideal and real gas simulations in the primary nozzle and mixing chamber for 0 mm primary nozzle position and 15 C evaporator temperature, (a) primary nozzle mass flow rate (b) MER

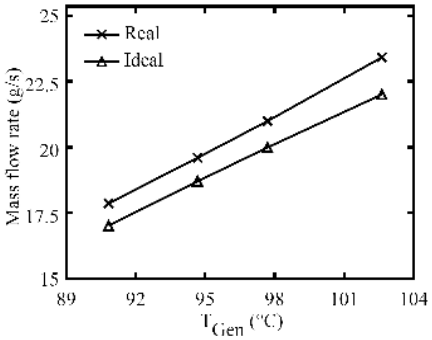

(a)

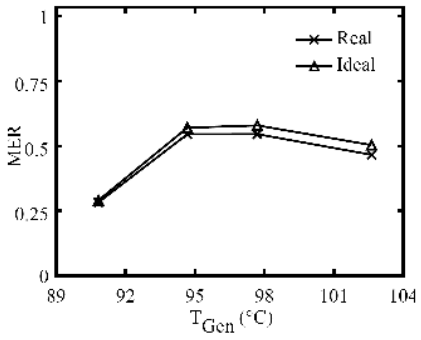

(b)

4 Conclusions

Numerical simulations of the flow in a vapour ejector have been carried out. In contrast to earlier numerical studies, all the calculations in the present study have utilised the real gas model for the refrigerant. Ejection (with the inlet from the evaporator blocked) as well as flow-through studies have been performed. In the former case, suction pressures corresponding to four different nozzle positions, namely, 0 mm, 18 mm, 30 mm and 36 mm, have been predicted and compared with experimental values reported by Yapici (2008). In the latter case, simulations have been carried out for three nozzle positions, 0 mm, 18 mm and 30 mm, four generator conditions, 91 C, 95 C, 98 C and 103 C and two evaporator conditions, 10 C and 15 C. The COP and MER have been evaluated for all the cases. The predicted COPs have been compared with experimental data.

Gas dynamics and fluid dynamics aspects of the flow, such as choking of the secondary flow, expansion of the primary jet and flow separation have been investigated in detail by tracking the sonic line and the edge of the primary stream. Such details have hitherto not been reported due to lack of optical access in the experimental setups, although in a recent work (Little and Garimella, 2016) have reported shadowgraph images of the flow of R134a in ejectors. In addition, earlier numerical simulations have mostly used air as the secondary fluid and not a refrigerant. The present study clearly demonstrates that it is not the choking of the secondary stream alone, as is currently believed, but the area available for the secondary stream affects the COP as well.

The ejection study predicts the lowest suction pressure for primary nozzle positions of 18 mm and 30 mm. When the nozzle is closer to the mixing chamber, lack of momentum transfer between the primary stream and entrained stream is shown to deteriorate the performance. At the farthest nozzle position studied (36 mm), primary stream expands prematurely inside the mixing chamber itself and thus blocks the entrained stream. The suction pressure is the lowest in nozzle positions in which both of the above effects are optimum. It is noteworthy that, none of the earlier numerical studies have predicted the suction pressure.

In the flow through study, both gas dynamic as well as fluid dynamic aspects of the flow field are used to draw inferences on the variation of the COP with generator temperature, evaporator temperature and primary nozzle position. It is found that there exists an optimum range of generator temperature for each nozzle position within which the COP attains a maximum. This is the range at which the mixing chamber area filled by the primary jet reaches a minimum. COP increases with an increase in the evaporator temperature for all the conditions studied. However, due to choking at higher generator conditions, rise in the COP is less than that at lower generator conditions. Increase in the distance between the primary nozzle and mixing chamber decreases the COP at lower generator temperatures due to the premature expansion of the primary stream inside the mixing chamber. In contrast, at higher generator temperatures, COP increases when the nozzle is pulled back. Here, due to choking, the primary stream expands to occupy the same cross-sectional area irrespective of the nozzle position. Owing to higher room for momentum transfer, the farthest nozzle position exhibits better performance at higher generator conditions.

For the range of operation and the refrigerant considered in the present study, deviation from ideal gas behaviour is shown to be significant in the primary nozzle but not very much so inside the mixing chamber. Real gas effects show only a moderate impact on the MER.

References

Arbel, A., Shklyar, A., Hershgal, D., Barak, M. and Sokolov, M. (2003) 'Ejector irreversibility characteristics', *Journal of Fluids Engineering*, Vol. 125, No. 1, pp.121–129.

Bartosiewicz, Y., Aiduon, Z., Desavaux, P. and Mercadier, Y. (2005) 'Numerical and experimental investigations on supersonic ejectors', *International Journal of Heat and Fluid Flow*, Vol. 26, No. 1, pp.56–70.

Chandra, V.V. and Ahmed, M.R. (2014) 'Experimental and computational studies on a steam jet refrigeration system with constant area and variable area ejectors', *Energy Conversion and Management*, Vol. 79, pp.377–386.

Chen, Z., Dang, C. and Hihara, E. (2017) 'Investigations on driving flow expansion characteristics inside ejectors', *International Journal of Heat and Mass Transfer*, Vol. 108, pp.490–500.

Hemidi, A., Henry, F., Leclaire, S., Seynhaeve, J-M. and Bartosiewicz, Y. (2009) 'CFD analysis of a supersonic air ejector. Part 1. Experimental validation of single-phase and two-phase operation', *Applied Thermal Engineering*, Vol. 29, No. 8, pp.1523–1531.

Hewedy, N.I.I., Hamed, M.H., Abou-Taleb, F.Sh. and Ghonim, T.A. (2008) 'Optimal performance and geometry of supersonic ejector', *Journal of Fluids Engineering*, Vol. 130, No. 4, pp.1–10.

Little, A.B. and Garimella, S. (2011) 'A review of ejector technology for refrigeration applications', *International Journal of Air-Conditioning and Refrigeration*, Vol. 19, No. 1, pp.1–15.

Little, A.B. and Garimella, S. (2016) 'Shadowgraph visualization of condensing R134a flow through ejectors', *International Journal of Refrigeration*, Vol. 68, No. 1, pp.118–129.

Little, A.B., Bartosiewicz, Y. and Garimella, S. (2015) 'Visualisation and validation of ejector flow field with computational and first-principles analysis', *Journal of Fluids Engineering*, Vol. 137, No. 5, pp.1–12.

Munday, J.T. and Bagster, D.F. (1977) 'A new ejector theory applied to steam jet refrigeration', *Industrial & Engineering Chemistry Process Design and Development*, Vol. 16, No. 4, pp.442–449.

Nahdi, E., Champoussin, J.C., Hostache, G. and Cheron, J. (1993) 'Optimal geometric parameters of a cooling ejector compressor', *International Journal of Refrigeration*, Vol. 16, No. 1, pp.67–72.

Ramesh, A.S. and Sekhar, S.J. (2018) 'Experimental studies on the effect of suction chamber angle on the entrainment of passive fluid in a steam ejector', *Journals of Fluids Engineering*, Vol. 140, No. 1, pp.1–8.

Shestopalov, K.O., Huang, B.J., Petrenko, V.O. and Volovyk, O.S. (2015) 'Investigation of an experimental ejector refrigeration machine operating with refrigerant R245fa at design and off-design working conditions. Part 1. Theoretical analysis', *International Journal of Refrigeration*, Vol. 55, pp.201–211.

Wilcox, D.C. (1994) *Turbulence Modeling for CFD*, 2nd ed., DCW industries, Inc., California.

Wu, H., Liu, Z., Han, B. and Li Y. (2014) 'Numerical investigation of the influences of mixing chamber geometries on steam ejector performance', *Desalination*, Vol. 353, pp.15–20.

Yapici, R. (2008) 'Experimental investigation of performance of vapor ejector refrigeration system using refrigerant R123', *Energy Conversion and Management*, Vol. 49, No. 5, pp.953–961.

Yapici, R. and Yetisen, C.C. (2007) 'Experimental study on ejector refrigeration system powered by low grade heat', *Energy Conversion and Management*, Vol. 48, No. 5, pp.1560–1568.

Younglove, B.A. and McLinden, M.O. (1994) 'an international standard equation of state for the thermodynamic properties of refrigerant 123 (2,2-Dichloro-1,1,1-Trifluoroethane)', *Journal of Physical and Chemical Reference Data*, Vol. 23, No. 5, pp.731–779.

Zheng, F., Kuznetsov, A.V. and Roberts, W.L. (2011) 'Influence of geometry on starting vortex and ejector performance', *Journal of Fluids Engineering*, Vol. 133, No. 5, pp.1–8.

Zhu, Y., Cai, W., Wen, C. and Li, Y. (2009) 'Numerical investigation of geometry parameters for design of high performance ejectors', *Applied Thermal Engineering*, Vol. 29, No. 5, pp.898–905.